A vehicle detector based on notched power for distributed acoustic sensing

Marco Fontana*, Ángel F. García-Fernández*†, Simon Maskell*
*Dept. of Electrical Engineering and Electronics, University of Liverpool, United Kingdom
†ARIES Research Centre, Universidad Antonio de Nebrija, Madrid, Spain
Emails: marco.fontana@liverpool.ac.uk, angel.garcia-fernandez@liverpool.ac.uk, s.maskell@liverpool.ac.uk

***Abstract*—Distributed acoustic sensing (DAS) has been shown to be a reliable tool for monitoring highways traffic in an efficient and cost-effective fashion. Nevertheless, multiple-lane highways and noise sources reduce the vehicle detection capabilities of DAS sensors, especially in high-traffic scenarios. In this paper, we propose a novel approach derived from harmonic analysis techniques to estimate vehicle trajectories from DAS data. Our method aims to detect closely-spaced lines by iteratively notching the contribution of the lines already estimated. The results show the remarkable performance of the proposed method compared to the Hough transform, proving the potential of the notched power vehicle detector in a wide range of noise levels.**

***Index Terms*—Distributed acoustic sensing (DAS), vehicle detector, line detector, notch periodogram.**

I. Introduction

In recent years, distributed acoustic sensing (DAS) has become one of the most promising solutions to provide effective and inexpensive monitoring systems for assets requiring long-distance continuous monitoring, e.g., highways, pipelines and borders [1]. DAS exploits Rayleigh scattering to turn an optical fibre deployed for telecommunication purposes into a sensing element, allowing to locate any dynamic strain induced by acoustic events with a meter-scale resolution [2], [3].

DAS-based systems have been deployed to detect and localise acoustic events such as pipeline leaks [4], [5], border intrusions [6], and utility poles [7]. Furthermore, several works already demonstrated the feasibility of DAS to detect traffic flow [8]–[11]. The layout of a typical DAS system includes an optical fibre cable deployed along the road, and an interrogator sending laser pulses from one end of the fibre. The output data is usually represented in a spatio-temporal map, often called a waterfall [12]. Fig. 1 reports an example of waterfall in a traffic monitoring scenario.

The high sensitivity, low-cost and low-maintenance requirements make DAS an attractive solution for traffic monitoring compared to other sensors, i.e. cameras, inductive loops, radars and wireless sensors [12]. The installation cost of DAS is lower compared to more traditional systems due to the ability to deploy the fibre in parallel with the road instead of above or under it and reuse existing telecommunication fibre as the sensing element of the system. Furthermore, DAS provides a spatial resolution of the order of meters without considerable infrastructure installed in or around the road, making the conventional traffic monitoring systems more expensive. Nevertheless, the optical fibre output is highly affected by cabling, soil condition, and proximity of noise sources, which lead to time-varying and position-dependent signal-to-noise ratio (SNR).

In the context of highway monitoring, the vehicle speed is almost constant in relatively short time periods and free traffic conditions. The vehicle trajectories usually appear as straight lines in the waterfall, where the spacing between the trajectories depends on the number of lanes and the traffic levels, see Fig. 1 for an example. Line detection methods represent a natural approach to obtain noise-resistant and consistent vehicle detections from the sensor's output.

Line detection has been traditionally performed by using the Hough Transform and its variations [13]–[15] to detect continuous straight edges in images, corresponding to physical phenomena [16], semantic lines [17] and geological features [18], among many others. The Hough transform has been used for traffic monitoring based on DAS data in [19], showing impressive performance in detecting trucks on the highway. Nevertheless, the approach has several limitations, as it struggles to detect low-intensity lines, close range vehicles and overlapping lines.

In this paper, we propose a new method to iteratively detect and estimate an unknown number of lines (representing vehicle trajectories) in the waterfall. The algorithm uses the concept of notch periodogram [20], [21] to iteratively remove the contribution of the lines in the objective function, allowing us to detect closely-spaced lines related to vehicles running next to each other on the highway. The proposed method is tested both on a synthetic and a real-world dataset, demonstrating remarkable performance even in low-SNR scenarios.

The remainder of the paper is organised as follows: Section II describes the proposed detector; Section III shows results and Section IV summarises our conclusions.

II. Notched power detector

A. DAS system model

We model a DAS system with C sensing units, also called channels, along a fibre sensor of length L. Each channel is indexed by $c \in \{1, 2, \ldots, C\}$ and is located at a fixed position $x_c = dc$, where d is the uniform distance between the channels.

At each time step k, each channel measures a noisy acoustic energy signal $y_c(k)$ that depends on the neighbouring vehicles,

This work is supported by Sintela Ltd.

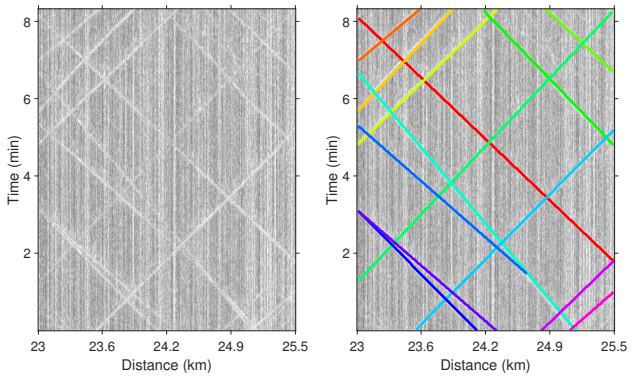

(a) DAS output (b) Vehicle trajectories

Figure 1: Example of a waterfall of 500 channels containing 14 vehicle trajectories. The x-axis represents the distance from the interrogator, while the y-axis shows the time.

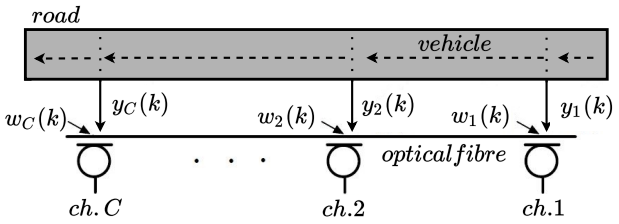

Figure 2: Schematic of the DAS system configuration in a traffic monitoring scenario. Each channel measures a noisy acoustic energy signal $y_i(t)$ from nearby vehicles.

as depicted in Fig. 2. The value of the signal $y_c(k)$ is represented by the pixel with coordinates (k, c) in Fig. 1, where each column shows a channel signal $\mathbf{y}_i$ in a short window of N time steps, and the entire image is the collection of C channel signals. We process the $N \times C$ acoustic energy matrix $\mathbf{Y} = [\mathbf{y}_1, \ldots, \mathbf{y}_C]$ expressed by the images of this kind, and we refer to them as waterfalls.

We aim to estimate an unknown number of vehicles trajectories in the waterfall, i.e., the parameters of the lines appearing in $\mathbf{Y}$. Assume the waterfall contains M lines, each of which is defined by a parameter $\theta_i \in \mathcal{A}$, where $\mathcal{A}$ is the parameter space. The entire set of lines is described by the vector of parameters $\boldsymbol{\theta} = [\theta_1, \ldots, \theta_M]^T$ we aim to estimate.

We model the channel signal $\mathbf{y}_c$ as a linear combination of $M + 1$ basis functions $\mathbf{g}_{\theta,c}$ associated to the channel c and defined by $\boldsymbol{\theta}$

$$\mathbf{y}_c = \mathbf{G}_{\boldsymbol{\theta},c}\mathbf{b}_c + \mathbf{w}_c \tag{1}$$

where $\mathbf{b}_c = [b_{c,0}, b_{c,1}, \ldots, b_{c,M}]^T$ is the unknown vector of amplitudes and $\mathbf{w}_c \in \mathbb{R}^N$ is a zero-mean additive white Gaussian noise (AWGN) with covariance matrix $\sigma_c^2 \boldsymbol{I}_{N\times N}$. The matrix

$$\mathbf{G}_{\boldsymbol{\theta},c} = [\mathbf{1}_{N\times 1}, \mathbf{g}_{\theta_1,c}, \ldots, \mathbf{g}_{\theta_M,c}]. \tag{2}$$

has dimensions $N \times (M + 1)$, and each column $i > 1$ is a basis function $\mathbf{g}_{\theta_i,c}$ evaluated at each point in the time series, and represents the line defined by the parameter θ_i at the distance x_c in the chosen time window. Each basis function $\mathbf{g}_{\theta_i,c}$ is defined by setting value to 1 at time point at which the modelled condition is defined, i.e., the vehicle is present, and 0 at all other time points. For example, if the vehicle is detected at the time instant k in the channel c, the corresponding basis function $\mathbf{g}_{\theta_i,c}$ is the standard basis $\boldsymbol{e}_k$ of the N-dimensional space of the channel signals, where the standard basis is defined such that $\mathbf{y}_c = \sum_{i=1}^{N} y_c(i)\boldsymbol{e}_i$.

B. Maximum likelihood estimation

Suppose M is known for now and the unknown parameter set is $\boldsymbol{\Theta}_M = \{\boldsymbol{\theta}, \mathbf{b}_{1:C}, \sigma^2_{1:C}\}$, where $\mathbf{b}_{1:C}$ and $\sigma^2_{1:C}$ are, respectively, the sets of amplitudes and noise variances over the C channels. Under the AWGN assumption, the log likelihood can be written as [22]

$$L^M(\boldsymbol{\Theta}_M) = \sum_{c=1}^{C}\left[-N\log\sigma_c - \frac{\|\mathbf{y}_c - \mathbf{G}_{\boldsymbol{\theta},c}\mathbf{b}_c\|^2}{2\sigma_c^2}\right] + C_L \tag{3}$$

where C_L is a constant term. To compute the maximum likelihood estimate (MLE), we seek to maximise (3) with respect to the parameter set $\boldsymbol{\Theta}_M$. Fixing $\boldsymbol{\theta}$ and $\mathbf{b}_{1:C}$, we can maximise with respect to σ_c^2 for each channel [22]

$$\widehat{\sigma}_c^2 = \frac{1}{N}\|\mathbf{y}_c - \mathbf{G}_{\boldsymbol{\theta},c}\mathbf{b}_c\|^2 . \tag{4}$$

Substituting (4) into (3), we obtain

$$\max_{\boldsymbol{\theta},\mathbf{b}_{1:C}} L^M(\boldsymbol{\theta}, \mathbf{b}_{1:C}, \widehat{\sigma}^2_{1:C}) = \min_{\boldsymbol{\theta},\mathbf{b}_{1:C}} \sum_{c=1}^{C}\frac{N}{2}\left[\log\left(\frac{1}{2}\|\mathbf{y}_c - \mathbf{G}_{\boldsymbol{\theta},c}\mathbf{b}_c\|^2\right) + 1\right] \tag{5}$$

$$= \min_{\boldsymbol{\theta},\mathbf{b}_{1:C}} J^M(\boldsymbol{\theta}, \mathbf{b}_{1:C}) \tag{6}$$

where

$$J^M(\boldsymbol{\theta}, \mathbf{b}_{1:C}) = \sum_{c=1}^{C}\log\left(\|\mathbf{y}_c - \mathbf{G}_{\boldsymbol{\theta},c}\mathbf{b}_c\|^2\right) \tag{7}$$

$$= \sum_{c=1}^{C} J_c^M(\boldsymbol{\theta}, \mathbf{b}_{1:C}) \tag{8}$$

is the sum of the log power of the estimated error signals $J_c^M(\cdot)$.

For a given $\boldsymbol{\theta}$, we can minimise (7)-(8) with respect to $\mathbf{b}_{1:C}$ by solving the least log squares problem for each channel c

$$\widehat{\mathbf{b}}_c = (\mathbf{G}^T_{\boldsymbol{\theta},c}\mathbf{G}_{\boldsymbol{\theta},c})^{-1}\mathbf{G}^T_{\boldsymbol{\theta},c}\mathbf{y}_c. \tag{9}$$

Substituting (9) in (7), we can rewrite the log likelihood, as a function of theta, for the optimal $\widehat{\mathbf{b}}_{1:C}$ and $\widehat{\sigma}^2_{1:C}$ as

$$S^M(\boldsymbol{\theta}) = J(\boldsymbol{\theta}, \widehat{\mathbf{b}}_{1:C}) = \sum_{c=1}^{C} S_c^M(\boldsymbol{\theta}) \tag{10}$$

where the log power of the estimated error signal is

$$S_c^M(\boldsymbol{\theta}) = \log\left(\left\|\mathbf{y}_c - \mathbf{G}_{\boldsymbol{\theta},\mathbf{c}}(\mathbf{G}^T_{\boldsymbol{\theta},c}\mathbf{G}_{\boldsymbol{\theta},c})^{-1}\mathbf{G}^T_{\boldsymbol{\theta},c}\mathbf{y}_c\right\|^2\right) . \tag{11}$$

Introducing the projection operators onto the span($\mathbf{G}_{\boldsymbol{\theta},c}$) and its orthogonal complement, respectively [23]

$$\mathbf{P}^{\parallel}_{\mathbf{G}_{\boldsymbol{\theta},c}} = \mathbf{G}_{\boldsymbol{\theta},c}(\mathbf{G}^T_{\boldsymbol{\theta},c}\mathbf{G}_{\boldsymbol{\theta},c})^{-1}\mathbf{G}^T_{\boldsymbol{\theta},c} \tag{12}$$

$$\mathbf{P}^{\perp}_{\mathbf{G}_{\boldsymbol{\theta},c}} = \boldsymbol{I} - \mathbf{P}^{\parallel}_{\mathbf{G}_{\boldsymbol{\theta},c}} = \boldsymbol{I} - \mathbf{G}_{\boldsymbol{\theta},c}(\mathbf{G}^T_{\boldsymbol{\theta},c}\mathbf{G}_{\boldsymbol{\theta},c})^{-1}\mathbf{G}^T_{\boldsymbol{\theta},c} \tag{13}$$

, we can rewrite the log power of the estimated error signal in (11) as

$$S^M_c(\boldsymbol{\theta}) = \log\left(\left\|\mathbf{y}_c - \mathbf{P}^{\parallel}_{\mathbf{G}_{\boldsymbol{\theta},c}}\mathbf{y}_c\right\|^2\right). \tag{14}$$

Thus, the parameter estimation is performed by minimising (10) over the parameter space $\mathcal{A}^M$. Each channel signal $\mathbf{y}_c$ contributes equally to the estimation of the global parameter $\boldsymbol{\theta}$, which represents a set of lines spanning through the C channels in the waterfall $\mathbf{Y}$.

C. Notched power

Assuming M is unknown, we proceed to minimise (10) iteratively. Suppose the vector of parameters $\boldsymbol{\theta}_v = [\theta_1, \dots \theta_r]$, $r < M$, is known from previous estimations; we refer to $\boldsymbol{\theta}_v$ as the notch vector. Assuming $\mathcal{A}$ is a finite alphabet of parameters, we aim to estimate the unknown parameter $\theta_i \in \mathcal{A}$ such that the estimated vector of parameters is the augmented set $\boldsymbol{\theta}_a = [\boldsymbol{\theta}_v, \theta_i]$.

The ML criterion for a model with $r+1$ parameters is given by [20]

$$S^{r+1}(\boldsymbol{\theta}_a) = \sum_{c=1}^{C} \log\left(\left\|\mathbf{y}_c - \mathbf{P}^{\parallel}_{\mathbf{G}_{\boldsymbol{\theta}_a,c}}\mathbf{y}_c\right\|^2\right) \tag{15}$$

$$= \sum_{c=1}^{C} \log\left(\exp S^r_c(\boldsymbol{\theta}_v) - P_{v,c}(\theta_i;\boldsymbol{\theta}_v)\right) \tag{16}$$

where

$$P_{v,c}(\theta_i;\boldsymbol{\theta}_v) = \left\|\mathbf{P}^{\parallel}_{\widetilde{\mathbf{g}}_{\theta_i,c}}\mathbf{y}_c\right\|^2 \tag{17}$$

is the notched power of the channel signal $\mathbf{y}_c$ with respect to the notch vector $\boldsymbol{\theta}_v$. The derivation of (16) is available in the appendix. The term $\mathbf{P}^{\parallel}_{\widetilde{\mathbf{g}}_{\boldsymbol{\theta}_i,c}}$ is the projector onto the space defined by the residual vector of $\mathbf{g}_{\boldsymbol{\theta}_i,c}$ onto span($\mathbf{G}_{\boldsymbol{\theta}_v,c}$)

$$\widetilde{\mathbf{g}}_{\theta_i,c} = \mathbf{P}^{\perp}_{\mathbf{G}_{\boldsymbol{\theta}_v,c}}\mathbf{g}_{\boldsymbol{\theta}_i,c} \tag{18}$$

such that $\widetilde{\mathbf{g}}_{\boldsymbol{\theta}_i,c} \perp$ span($\mathbf{G}_{\boldsymbol{\theta}_v,c}$). We define the objective function $F^{r+1}(\cdot)$ as

$$F^{r+1}(\boldsymbol{\theta}_a) = -\frac{S^{r+1}(\boldsymbol{\theta}_a)}{d_T(\theta_i)} \tag{19}$$

where $d_T(\theta_i)$ is the number of channels in which the trajectory θ_i is supposed to exist. The parameter estimation is performed by maximising the objective function

$$\arg\max_{\theta_i \in \mathcal{A}} F^{r+1}(\boldsymbol{\theta}_a) = \arg\max_{\theta_i \in \mathcal{A}} -\frac{S^{r+1}(\boldsymbol{\theta}_a)}{d_T(\theta_i)} = \widehat{\theta}_i\,. \tag{20}$$

If we assume that $\boldsymbol{\theta}_v$ is the optimal value of of the previous estimations, the lines corresponding to the parameters $\boldsymbol{\theta}_v$ are notched, and thus contribute nothing to the notched power. Note that the proposed approach performs an estimation of the global of parameters $\boldsymbol{\theta}$ by modelling and notching each channel signal independently.

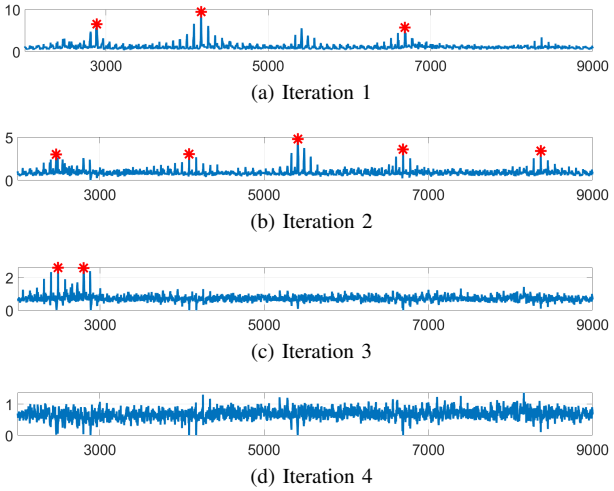

Figure 3: Evolution of the notched power throughout the estimation process. The red markers represent the estimated parameters in the alphabet $\mathcal{A}$ at each iteration.

D. Iterative parameter estimation

The log power of the estimated error signal (16) can be iteratively computed on the subset of parameters defined by $\boldsymbol{\theta}_v$ to detect the trajectories in the waterfall, as detailed in Alg. 1.

Assuming the average speed of the vehicles on the highway is known, we can efficiently compute the channel notched power (17) by defining $\mathbf{G}_{\boldsymbol{\theta},c}$ on a finite alphabet $\mathcal{A}$ of candidate parameters, such that $\theta_i \in \mathcal{A}$. The local maxima of the objective function (20) are then used to estimate a set of candidate parameters $\widetilde{\boldsymbol{\theta}}_i$.

Fig. 3 shows the notched power evaluated at each iteration in the alphabet $\mathcal{A}$. The parameters estimated at the first iteration are represented by red markers in Fig. 3a, and their contribution to the notched power is zero at second iteration, as shown in Fig. 3b. The same applies to the subsequent iterations, until the objective function $F^{r+1}(\cdot)$ shows no relevant peaks. The algorithm terminates when the value of one of the detected peaks is below the threshold Γ_P, which is defined on the mean value of the objective function $F^{r+1}(\cdot)$ at the current estimation.

The local maxima of the objective function are due to the sum of the contributions from several basis functions, with peaks related mainly to noise or partially overlapping trajectories. We consider the subset of the candidate parameters $\bar{\boldsymbol{\theta}}_i \subset \widetilde{\boldsymbol{\theta}}_i$ that gives the greatest contribution in the objective function by the following procedure.

To reduce the number of false target detections, it is convenient to cluster the candidate parameters $\widetilde{\boldsymbol{\theta}}_i$ based on their mutual orthogonality, such that each of the basis function $\mathbf{g}_{\theta_i,c}$ of a cluster is approximately orthogonal to the basis functions belonging to the other clusters. The preliminary set of estimated parameters $\bar{\boldsymbol{\theta}}_i$ at the current iteration is defined by the maximum of the objective function evaluated on the subset of parameters in each cluster.

As the evaluation of the objective function is computationally expensive, we estimate the parameters in two steps based on different alphabets. The first step evaluates the

Algorithm 1 Notched power detector

Input: $\{\mathbf{y}, \mathcal{A}, \alpha_i\}$ **Output:** $\{\boldsymbol{\theta}_a\}$

$\boldsymbol{\theta}_a \leftarrow \{\}$
$r = 0$
$\mathbf{P}_c^{\parallel} \leftarrow \mathbf{0}_{N\times N}$, $\forall c \in \{1, 2, \ldots, C\}$
do
  $\boldsymbol{\theta}_v \leftarrow \boldsymbol{\theta}_a$
  for all channels $c \in \{1, 2, \ldots, C\}$ **do**
    for all parameters $\theta_i \in \mathcal{A}$ **do**
      $\widetilde{\mathbf{g}}_{\boldsymbol{\theta}_i,c} \leftarrow \mathbf{P}^{\perp}_{\mathbf{G}_{\boldsymbol{\theta}_v,c}} \mathbf{g}_{\boldsymbol{\theta}_i,c}$
      $P_{v,c}(\theta_i; \boldsymbol{\theta}_v) \leftarrow \left\| \mathbf{P}^{\parallel}_{\widetilde{\mathbf{g}}_{\boldsymbol{\theta}_i,c}} \mathbf{y}_c \right\|^2$
    end for
  end for
  $S^{r+1}([\boldsymbol{\theta}_v, \theta_i]) \leftarrow \sum_{c=1}^{C} \log\left(\exp S_c^r(\boldsymbol{\theta}_v) - P_{v,c}(\theta_i; \boldsymbol{\theta}_v)\right)$
  $F^{r+1} \leftarrow -S^{r+1}([\boldsymbol{\theta}_v, \theta_i])/d_T(\theta_i)$
  if $F^{r+1}([\boldsymbol{\theta}_v, \theta_i]) < \Gamma_P$ **then**
    $\bar{\boldsymbol{\theta}}_i \leftarrow$ local maxima of $F^{r+1}([\boldsymbol{\theta}_v, \theta_i])$
    $\{\bar{\boldsymbol{\theta}}_{i,q}\}_{q\in\{1,\ldots,Q\}} \leftarrow Q$ clusters of $\bar{\boldsymbol{\theta}}_i$
    for all clusters $q \in \{1, \ldots, Q\}$ **do**
      $\bar{\theta}_{i,q} \leftarrow \arg\max_{\theta_i \in \widetilde{\boldsymbol{\theta}}_{i,q}} F^{r+1}([\boldsymbol{\theta}_v, \theta_i])$
      $\widehat{\theta}_i \leftarrow \arg\max_{\theta_i \in \mathcal{B}_{\bar{\theta}_{i,q}}} F^{r+1}([\boldsymbol{\theta}_v, \theta_i])$
    end for
    for all parameters $\theta_i \in \widehat{\boldsymbol{\theta}}_i$ **do**
      for all channels $c \in \{1, 2, \ldots, C\}$ **do**
        $\mathbf{P}_c^{\parallel} = \mathbf{P}_c^{\parallel} + \mathbf{P}^{\parallel}_{\widetilde{\mathbf{g}}_{\widehat{\theta}_i,c}}$
      end for
    end for
    $\boldsymbol{\theta}_a \leftarrow \{\boldsymbol{\theta}_v, \widehat{\boldsymbol{\theta}}_i\}$
    $r \leftarrow r + size(\widehat{\boldsymbol{\theta}}_i)$
  end if
while $F^{r+1}([\boldsymbol{\theta}_v, \theta_i]) > \Gamma_P$

objective function on a relatively sparse alphabet $\mathcal{A}$, and allows us to efficiently obtain a preliminary set of estimated parameters $\bar{\boldsymbol{\theta}}_i$. The second step refines the estimation of each parameter $\bar{\theta}_i \in \bar{\boldsymbol{\theta}}_i$ by recomputing the objective function on a denser dataset $\mathcal{B}_{\bar{\theta}_i}$ centred on $\bar{\theta}_i$, such that $\mathcal{B}_{\bar{\theta}_i} \cap \mathcal{A} = \{\bar{\theta}_i\}$. This procedure improves the accuracy of the estimations and reduces the false target error, as the notched power manages to suppress the components of the detected lines with a greater precision.

The resulting parameters $\widehat{\boldsymbol{\theta}}_i$ are used to define the basis functions $\widetilde{\mathbf{g}}_{\widehat{\theta}_i,c}$ as in (18) and extend the space of the detected lines. Note that it is possible to model the width w_i of the detected lines by defining the associated basis function as a linear combination of the standard basis $\boldsymbol{e}_j$ of the N-dimensional space of the channel signals

$$\mathbf{g}_{\theta_i,c} = \sum_{j=k_c-\frac{w_i-1}{2}}^{k_c+\frac{w_i-1}{2}} \boldsymbol{e}_j \tag{21}$$

where $k_c \in [1, N]$ is the time instant at which the line is detected in the channel c and w_i is odd.

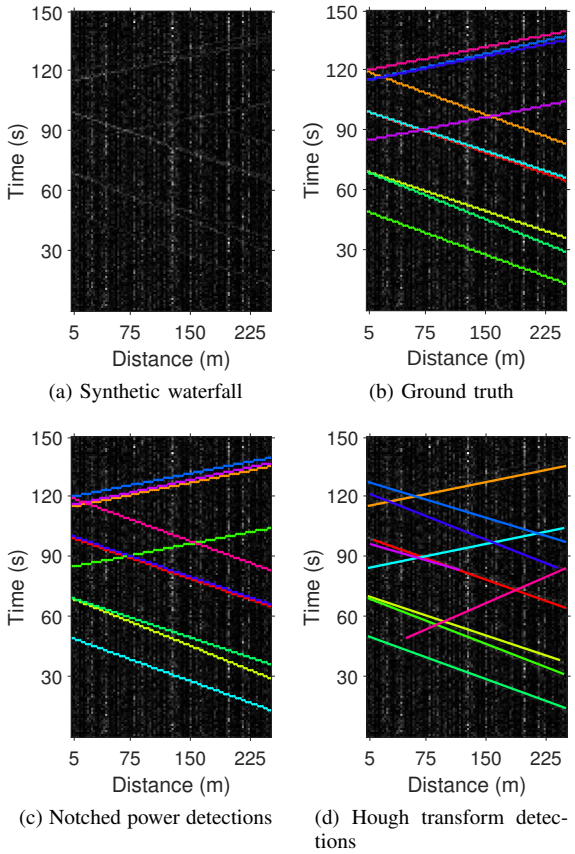

(a) Synthetic waterfall (b) Ground truth

(c) Notched power detections (d) Hough transform detections

Figure 4: Synthetic waterfall with $\text{SNR}_c = -5$ dB.

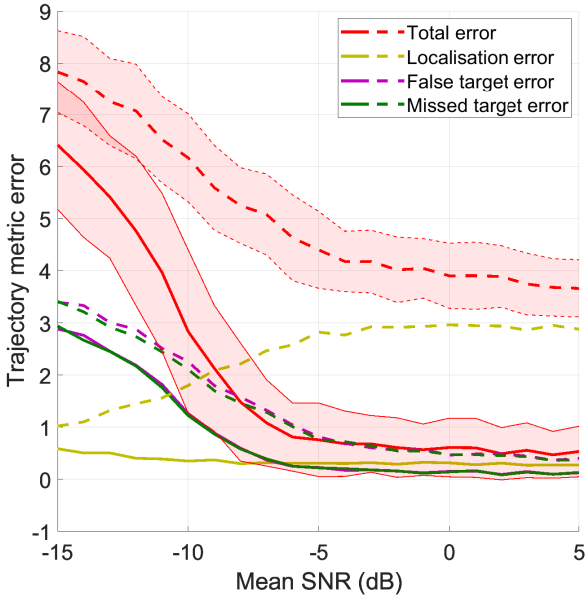

Figure 5: Performance comparison between vehicle detector based on notched power (solid lines) and Hough transform (dotted lines), averaged on 100 synthetic waterfalls for several noise levels. The coloured areas represent the standard deviation from the mean value.

III. Experimental evaluation

In this section, we evaluate the proposed method both on a synthetic and a real-world dataset. In both cases, we report the performance by means of the metric for sets of trajectories [24] with parameters $c = 5$ m, $p = 1$, and $\gamma = 1$. The trajectory metric error measures localisation error, missed and false target errors, and track switching. The Matlab implementation of the proposed algorithm has been tested on a laptop equipped with Intel (R) Core(TM) i7-8850H @ 2.60 GHz and 16 GB of memory.

1) Evaluation on a synthetic dataset: First, we evaluate the performance of the proposed vehicle detector on a dataset of 100 synthetic waterfalls with $C = 100$ channels and $N = 150$ data points. We assume that we know that each waterfall contains the trajectories of $M = 10$ vehicles in both directions of travel, and the vehicle speed in each direction is assigned according to a Gaussian distribution of mean $\overline{v}_1 = 50$ km/h or $\overline{v}_2 = 90$ km/h and standard deviation $\sigma_1 = \sigma_2 = 5$ km/h. The finite alphabet $\mathcal{A}$ is the union of two sub-alphabets $\mathcal{A}_1$ and $\mathcal{A}_2$ centred on $\overline{v}_1$ and $\overline{v}_2$, respectively; each sub-alphabet $\mathcal{A}_i$ represents lines of slope $m \in \{\overline{v}_i - 7, \overline{v}_i - 6, \ldots, \overline{v}_i + 7\}$ and offset $b_L \in [1, N]$. Each trajectory i has a signal power $P_i \in [2, 5]$, and the SNR in each channel is assigned according to a Gaussian distribution of mean SNR_c and standard deviation $\sigma_w = 5$ dB.

Fig. 4a shows an example of synthetic waterfall for $\text{SNR}_c = -5$ dB, and the related ground truth is depicted in Fig. 4b. The scenario is designed to provide closely-spaced lines representing vehicles running next to each other on the highway, potentially on different lanes. The lines resulting from the parameters estimation are shown in Fig. 4c, where the colour map reflects the order of detection, and it is irrelevant in this context.

We compared the proposed method with a detector based on the Hough transform [13] and Roberts cross edge detector [25]. The threshold Γ_E of the edge detector has been set to $\Gamma_E = 0.12$, while the spacing of Hough transform bins was $d_H = 0.7$. Both Γ_E and d_H have been determined by minimising the false and missed target errors for all the noise levels evaluated in the simulation. We consider the peaks of the Hough transform in a range $\theta_H \in [65, 85]$ degrees with resolution $d_{\theta_H} = 0.5$ degrees; the selected range expresses the average speed of the vehicles on the highway, which is supposed to be known. The peaks are selected among those exceeding the 30% of the maximum of the Hough transform, and suppression neighbourhoods of dimensions 11×11 around each identified peak have been set to avoid double detections in the Hough transform matrix.

The mean total trajectory metric and its standard deviation is reported in red in Fig. 5 for both the notched power and Hough transform detectors, along with its components. Note that the track switching error is not displayed because it is negligible. The total error of the Hough transform detector has a trend similar to the total notched power detector error, but it results considerably larger for all the noise levels. The error composition is quite different among the detectors, as the main contribution for the Hough transform detector is due to the localisation error, while the notched power detector shows a very low error of this kind for all the noise levels evaluated. False and missed target errors appear to be highly correlated for both the detectors, with particularly low values in the range $\text{SNR}_c \in [-5, 5]$ dB. Again, the notched power detector shows better performance than the Hough transform detector for all the noise levels. The proposed detector runs for an average number of 2.67 iterations, and the mean execution time per iteration is 7.52 s.

Table I: Performance comparison between notched power detector and Hough transform detector based on the real dataset.

		Trajectory metric error			
		Total	Localization	False Target	Missed Target
Mean	Notched power	15.62	6.52	5.16	3.94
	Hough transform	20.99	6.65	7.69	6.65
Std. deviation	Notched power	6.34	2.22	3.48	2.39
	Hough transform	8.02	2.82	4.1	3.02

2) Evaluation on a real dataset: We process data from a DAS system deployed along a 28-km long highway. The system provides 4431 channel signals spaced of 6.38 m at a data-rate of 4 Hz. We consider a dataset of 36 waterfalls with $C = 256$ channels and $N = 128$ data points. Each waterfall contains an average of 9 trajectories and it is recoded by the system on one of the two different sets of channels selected for this evaluation. Fig. 6a and 6b show an example of waterfall in the dataset, where the ground truth in Fig. 6b has been manually generated by visual inspection.

We have adjusted the parameters of the notched detector to deal with the real data set. The alphabet $\mathcal{A}$ of the notched power detector has been defined on lines with slopes corresponding with the speed range $v \in \pm[55, 125]$ km/h, and the range of θ_H has been set to $\theta_H \in \pm[15, 45]$. For the Hough transform detector, the threshold Γ_E of the edge detector has been lowered to $\Gamma_E = 0.09$ to allow more points to be used as input of the transform. An example of the edge detector's output is reported in Fig. 6d.

To reduce the likelihood of multiple detections of the same line, we set a constant line width to $w_i = 23$ for the notched power detector, and we increased the suppression neighbourhoods up to 79×29 in the Hough transform matrix.

Tab. I compares the performance of the two detectors, with the notched power detector outperforming the Hough transform detector in terms of total error and in its single components. As in the previous experiment, the track switching error is not reported because it is negligible. The error is higher compared to the synthetic dataset due to a more complex noise pattern and the non-uniform width of the trajectories. Moreover, the wider range of possible slopes increases the chance of multiple detections of the same trajectory for both the detectors. An example of this type can be observed in Fig. 6e, where one of the trajectories has been detected three times, each time with a different slope.

IV. Conclusions

In this paper, we have presented a novel approach for vehicle detection suitable for DAS data. The method is based on

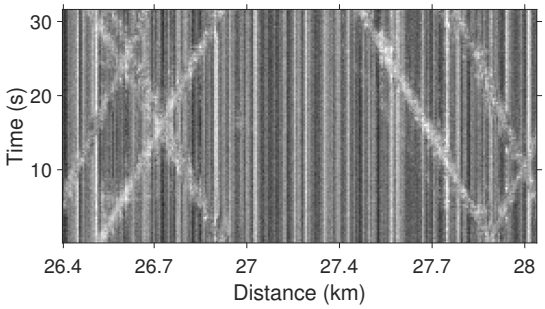

(a) Original waterfall

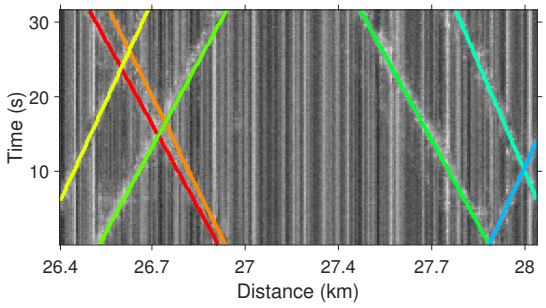

(b) Ground truth

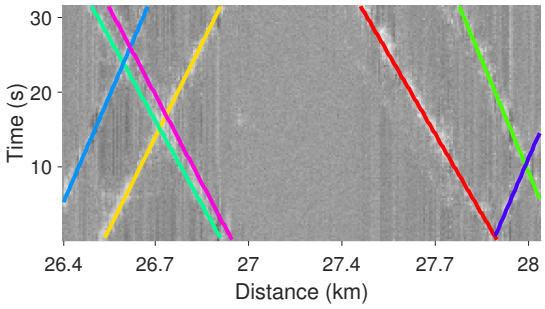

(c) Notched power detections on normalised waterfall

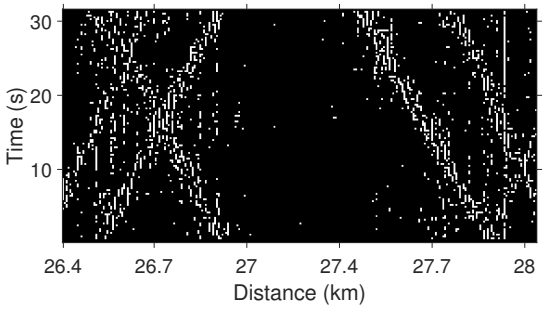

(d) Output of edge detection

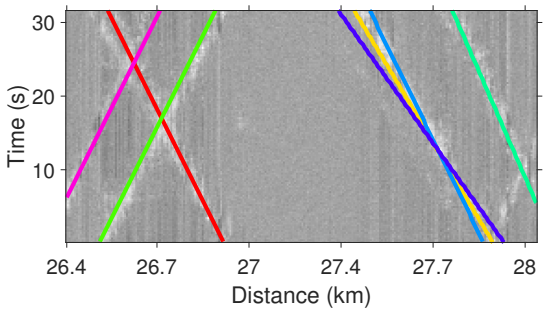

(e) Hough transform detections on normalised waterfall

Figure 6: Example of trajectory detection in the real dataset.

an iterative procedure that removes the contribution of the detected vehicle's trajectories in the notched power, which is evaluated on a finite alphabet of parameters. We have described a procedure to estimate multiple parameters from a single evaluation of the notched power, refining each estimation on a denser alphabet. The comparison of the algorithm performance with a detector based on the Hough transform shows greater accuracy in terms of localisation, false targets and missed targets with both the synthetic and the real datasets.

Although the execution time of the notched power detector is considerably higher than the Hough transform detector, the proposed algorithm managed to detect vehicles in real-time in both datasets, assuming a data rate of 4 Hz. Nevertheless, future work will focus on improving computational time and performance by estimating the width of the lines and refining the criteria to determine the number of trajectories.

Notched power

Assume the notch vector $\boldsymbol{\theta}_v$ of r parameters estimated in the previous iterations, and consider the augmented set $\boldsymbol{\theta}_a = [\boldsymbol{\theta}_v, \theta_i]$ with the correspondent basis function $\mathbf{G}_{\boldsymbol{\theta}_a,c}$ in the channel c. Let $\widetilde{\mathbf{g}}_{\theta_i,c} = \mathbf{P}^{\perp}_{\mathbf{G}_{\boldsymbol{\theta}_v,c}} \mathbf{g}_{\theta_i,c}$ be the residual vector, s.t. $\widetilde{\mathbf{g}}_{\theta_i,c} \perp \text{span}(\mathbf{G}_{\theta_i,c})$. The projection matrix of $\mathbf{G}_{\boldsymbol{\theta}_a,c}$ can be decomposed as

$$\mathbf{P}^{\parallel}_{\mathbf{G}_{\boldsymbol{\theta}_a,c}} = \mathbf{P}^{\parallel}_{\mathbf{G}_{\boldsymbol{\theta}_v,c}} + \widetilde{\mathbf{g}}_{\theta_i,c} (\widetilde{\mathbf{g}}^T_{\theta_i,c} \widetilde{\mathbf{g}}_{\theta_i,c})^{-1} \widetilde{\mathbf{g}}^T_{\theta_i,c} \tag{22}$$

Consider the notch power of the channel signal $\mathbf{y}_c$ with respect to the parameter $\boldsymbol{\theta}_v$

$$S^r_c(\boldsymbol{\theta}_v) = \log \left(\left\| \mathbf{y}_c - \mathbf{P}^{\parallel}_{\mathbf{G}_{\boldsymbol{\theta}_v,c}} \mathbf{y}_c \right\|^2 \right) \tag{23}$$

$$= \log \left(\|\mathbf{y}_c\|^2 - \left\| \mathbf{P}^{\parallel}_{\mathbf{G}_{\boldsymbol{\theta}_v,c}} \mathbf{y}_c \right\|^2 \right) . \tag{24}$$

Inserting (22) in (24), we can rewrite the sum of the log power of the estimated error signals $S^{r+1}(\boldsymbol{\theta}_a)$. Noting that the two terms in (22) are projectors associated with two orthogonal subspaces [20], we have

$$S^{r+1}(\boldsymbol{\theta}_a) = \sum_{c=1}^{C} \log \left(\|\mathbf{y}_c\|^2 - \left\| \mathbf{P}^{\parallel}_{\mathbf{G}_{\boldsymbol{\theta}_v,c}} \mathbf{y}_c \right\|^2 \right. \tag{25}$$

$$\left. - \left\| \widetilde{\mathbf{g}}_{\theta_i,c} (\widetilde{\mathbf{g}}^T_{\theta_i,c} \widetilde{\mathbf{g}}_{\theta_i,c})^{-1} \widetilde{\mathbf{g}}^T_{\theta_i,c} \mathbf{y}_c \right\|^2 \right) \tag{26}$$

$$= \sum_{c=1}^{C} \log \left(\exp S^r_c(\boldsymbol{\theta}_v) - \left\| \mathbf{P}^{\parallel}_{\widetilde{\mathbf{g}}_{\theta_i,c}} \mathbf{y}_c \right\|^2 \right) . \tag{27}$$

References

[1] Y. Wang, H. Yuan, X. Liu, Q. Bai, H. Zhang, Y. Gao, and B. Jin, "A comprehensive study of optical fiber acoustic sensing," *IEEE Access*, vol. 7, pp. 85 821–85 837, 2019.

[2] L. Palmieri, "Distributed optical fiber sensing based on Rayleigh scattering," *The Open Optics Journal*, vol. 7, no. 1, pp. 104–127, 2013.

[3] A. Masoudi and T. P. Newson, "Contributed review: Distributed optical fibre dynamic strain sensing," *Review of Scientific Instruments*, vol. 87, no. 1, p. 011501, Jan. 2016.

[4] C. Wang, M. Olson, B. Sherman, N. Dorjkhand, J. Mehr, and S. Singh, "Reliable leak detection in pipelines using integrated DdTS temperature and DAS acoustic fiber-optic sensor," in *2018 International Carnahan Conference on Security Technology (ICCST)*. IEEE, Oct. 2018.

[5] J. Zuo, Y. Zhang, H. Xu, X. Zhu, Z. Zhao, X. Wei, and X. Wang, "Pipeline leak detection technology based on distributed optical fiber acoustic sensing system," *IEEE Access*, vol. 8, pp. 30 789–30 796, 2020.

[6] H. Wu, Z. Wang, F. Peng, Z. Peng, X. Li, Y. Wu, and Y. Rao, "Field test of a fully distributed fiber optic intrusion detection system for long-distance security monitoring of national borderline," in *23rd International Conference on Optical Fibre Sensors*. SPIE, Jun. 2014.

[7] Y. Lu, Y. Tian, S. Han, E. Cosatto, S. Ozharar, and Y. Ding, "Automatic fine-grained localization of utility pole landmarks on distributed acoustic sensing traces based on bilinear resnets," in *ICASSP 2021 - 2021 IEEE International Conference on Acoustics, Speech and Signal Processing (ICASSP)*. IEEE, Jun. 2021.

[8] E. Martin, N. Lindsey, S. Dou, J. Ajo-Franklin, T. Daley, B. Freifeld, M. Robertson, C. Ulrich, A. Wagner, and K. Bjella, "Interferometry of a roadside DAS array in fairbanks, AK," in *SEG Technical Program Expanded Abstracts 2016*. Society of Exploration Geophysicists, Sep. 2016.

[9] H. Liu, J. Ma, T. Xu, W. Yan, L. Ma, and X. Zhang, "Vehicle detection and classification using distributed fiber optic acoustic sensing," *IEEE Transactions on Vehicular Technology*, vol. 69, no. 2, pp. 1363–1374, Feb. 2020.

[10] M.-F. Huang, P. Ji, T. Wang, Y. Aono, M. Salemi, Y. Chen, J. Zhao, T. J. Xia, G. A. Wellbrock, Y.-K. Huang, G. Milione, and E. Ip, "First field trial of distributed fiber optical sensing and high-speed communication over an operational telecom network," *Journal of Lightwave Technology*, vol. 38, no. 1, pp. 75–81, Jan. 2020.

[11] M. v. d. Ende, A. Ferrari, A. Sladen, and C. Richard, "Deep Deconvolution for Traffic Analysis with Distributed Acoustic Sensing Data," Sep. 2021.

[12] H. Liu, J. Ma, W. Yan, W. Liu, X. Zhang, and C. Li, "Traffic flow detection using distributed fiber optic acoustic sensing," *IEEE Access*, vol. 6, pp. 68 968–68 980, 2018.

[13] R. O. Duda and P. E. Hart, "Use of the Hough transformation to detect lines and curves in pictures," *Communications of the ACM*, vol. 15, no. 1, pp. 11–15, Jan. 1972.

[14] L. A. Fernandes and M. M. Oliveira, "Real-time line detection through an improved Hough transform voting scheme," *Pattern Recognition*, vol. 41, no. 1, pp. 299–314, Jan. 2008.

[15] R. Jošth, M. Dubská, A. Herout, and J. Havel, "Real-time line detection using accelerated high-resolution Hough transform," in *Image Analysis*. Springer Berlin Heidelberg, 2011, pp. 784–793.

[16] Y. Zhang, S. Fang, C. Lin, J. Zhang, C. Jiang, Y. Zeng, F. Huang, and H. Miao, "A new method for locating Kikuchi bands in electron backscatter diffraction patterns," *Microscopy Research and Technique*, vol. 82, no. 12, pp. 2035–2041, 2019.

[17] K. Zhao, Q. Han, C.-B. Zhang, J. Xu, and M.-M. Cheng, "Deep Hough Transform for Semantic Line Detection," *IEEE Transactions on Pattern Analysis and Machine Intelligence*, pp. 1–1, 2021.

[18] N. C. Fitton and S. J. D. Cox, "Optimising the application of the Hough transform for automatic feature extraction from geoscientific images," *Computers & Geosciences*, vol. 24, no. 10, pp. 933–951, Dec. 1998.

[19] C. Wiesmeyr, C. Coronel, M. Litzenberger, H. J. Döller, H.-B. Schweiger, and G. Calbris, "Distributed Acoustic Sensing for Vehicle Speed and Traffic Flow Estimation," in *2021 IEEE International Intelligent Transportation Systems Conference (ITSC)*, 2021.

[20] J. K. Hwang and Y.-C. Chen, "Superresolution frequency estimation by alternating notch periodogram," *IEEE Transactions on Signal Processing*, vol. 41, no. 2, pp. 727–741, 1993.

[21] M. Macleod, "A fast frequency domain notch periodogram algorithm," *Signal Processing*, vol. 81, no. 7, pp. 1449–1463, Jul. 2001.

[22] J.-K. Hwang and Y.-C. Chen, "A combined detection-estimation algorithm for the harmonic-retrieval problem," *Signal Processing*, vol. 30, no. 2, pp. 177–197, Jan. 1993.

[23] C. R. R. Christian Heumann and H. T. Shalabh, *Linear Models and Generalizations*. Springer Berlin Heidelberg, 2010.

[24] Á. F. García-Fernández, A. S. Rahmathullah, and L. Svensson, "A metric on the space of finite sets of trajectories for evaluation of multi-target tracking algorithms," *IEEE Transactions on Signal Processing*, vol. 68, pp. 3917–3928, 2020.

[25] L. S. Davis, "A survey of edge detection techniques," *Computer Graphics and Image Processing*, vol. 4, no. 3, pp. 248–270, Sep. 1975.